

Revisiting last glacial maximum climate over China and East Asian monsoon using PMIP3 simulations



Zhiping Tian^{a,*}, Dabang Jiang^{a,b,c}

^a Institute of Atmospheric Physics, Chinese Academy of Sciences, Beijing, China

^b CAS Center for Excellence in Tibetan Plateau Earth Sciences, Beijing, China

^c Collaborative Innovation Center on Forecast and Evaluation of Meteorological Disasters, Nanjing University of Information Science & Technology, Nanjing, China

ARTICLE INFO

Article history:

Received 30 November 2015

Received in revised form 22 March 2016

Accepted 6 April 2016

Available online 11 April 2016

Keywords:

Last glacial maximum

Climate over China

East Asian monsoon

PMIP3 simulations

ABSTRACT

Using simulations performed by all available climate models participating in the latest Paleoclimate Modelling Intercomparison Project (PMIP) phase 3 (PMIP3), we revisited the climate over China and the East Asian monsoon during the last glacial maximum (LGM; 21,000 years ago). Similar to previous results obtained from the PMIP phases 1 and 2 (PMIP1/2) models, all nine models reproduced colder than the pre-industrial annual and seasonal temperatures over China during the LGM and underestimated the annual cooling as evidenced by proxy data. The LGM annual and seasonal precipitation and evaporation over China consistently decreased in the models, whereas the very small LGM change in net precipitation (precipitation minus evaporation) differed among models. The annual net precipitation change during the LGM was broadly consistent with reconstructed moisture conditions over most parts of China, especially over the western Tibetan Plateau where the PMIP1/2 models disagreed with the proxy data. Moreover, the LGM winter monsoon circulation weakened (strengthened) over the East Asian continent in four (one) of five models; the summer monsoon circulation generally weakened in two models, whereas it weakened north and strengthened south of about 30°N over East Asia in three models. The spatial patterns of the LGM change in East Asian winter and summer monsoons in the PMIP3 models differed somewhat from those in the PMIP1/2 simulations.

© 2016 Elsevier B.V. All rights reserved.

1. Introduction

The last glacial maximum (LGM), around 21,000 years ago, refers to the interval of extremely cold and dry conditions during the last glacial period (Bartlein et al., 2011), when the global volume of ice sheets was at its greatest and the reconstructed global mean surface temperature was 3–8 K lower than the pre-industrial level (Masson-Delmotte et al., 2013). The LGM helps to understand the Earth system response to relatively well-defined radiative perturbations linked to large ice sheets and lower atmospheric concentrations of greenhouse gases (Masson-Delmotte et al., 2013).

Numerous reconstructions and simulations have been performed to examine the LGM climate at global and regional scales. In the East Asian monsoon region, atmospheric general circulation models (AGCMs) were initially used to address the climate during the LGM (Wang and Zeng, 1993; Yu et al., 2001; Liu et al., 2002; Jiang et al., 2003; Zhao et al., 2003), followed by regional climate models nested within AGCMs (Zheng et al., 2004; Ju et al., 2007). In the framework of the Paleoclimate Modelling Intercomparison Project (PMIP; Jousaume and Taylor, 1995), AGCMs either with prescribed sea surface temperatures

(SST-f) or coupled with slab ocean models (SST-c) within the PMIP phase 1 (PMIP1) and coupled atmosphere–ocean general circulation models (AOGCMs) or atmosphere–ocean–vegetation general circulation models (AOVGCMs) within the PMIP phase 2 (PMIP2) were used to simulate the LGM climate over East Asia (Yanase and Abe-Ouchi, 2007; Zhou and Zhao, 2009; Jiang and Lang, 2010; Jiang et al., 2011). These studies revealed that climate models are capable of reproducing the generally colder and drier climate and large-scale changes in atmospheric circulation over East Asia during the LGM despite the large scatter in the simulated magnitude and spatial pattern and uncertainties among models. In recent years, many climate models of variable complexity have been developed; however, what the LGM climate over East Asia was remains unclear when latest models are used. Hence, it is necessary to analyze similarities and differences among numerical experiments from the perspective of multiple climate models at different stages.

In addition to the abovementioned uncertainties among climate models, there are discrepancies between simulations and proxy data for the LGM climate change over East Asia. Using all 24 models for the LGM climate simulations, including 17 PMIP1 AGCMs with SST-f or SST-c plus seven PMIP2 AOGCMs and AOVGCM (hereafter collectively referred to as coupled models), Jiang et al. (2011) examined the LGM climate over China and compared simulations with multiproxy data. They found that previous models successfully reproduced the surface

* Corresponding author.

E-mail address: tianzhiping@mail.iap.ac.cn (Z. Tian).

cooling trend but generally underestimated the reconstructed cooling magnitude over China during that period, especially over the Hexi Corridor and North and Northeast China. In addition, the surface cooling magnitude better agreed with the proxy data in simulations with computed SSTs (including PMIP1 SST-c AGCMs and PMIP2 coupled models) than with prescribed SSTs (PMIP1 SST-f AGCMs). On the other hand, the simulated large-scale change in net precipitation agreed qualitatively with the moisture conditions reconstructed from lake status data over China despite the disagreements at the sub-regional scale, such as over the Tibetan Plateau (Jiang et al., 2011). Moreover, the simulations with computed (prescribed) SSTs were consistent (inconsistent) with reconstructed moisture conditions over most parts of West China except the Tibetan Plateau. Note that more than half of the above climate models were AGCMs, in which the important role of ocean dynamics was not included and thus there was lack of interaction between the atmosphere and ocean. Therefore, to what extent the latest coupled models are compatible with the proxy data over China during the LGM needs to be reexamined. Furthermore, the spatial coverage of the earlier records used to reconstruct the LGM climate over China is very sparse, which hampers the thorough model–data comparison and encourages the compilation of more reconstruction records with multiple proxies.

Relative to previous phases, the latest PMIP phase 3 (PMIP3) or Coupled Model Intercomparison Project phase 5 (CMIP5) comprises models that are more comprehensive, a broader set of experiments, higher spatial resolution models, a richer archive of output fields, and better documentation of the models and experiment conditions than earlier phases (Taylor et al., 2012). Thus, revisiting the LGM climate over East Asia using the latest PMIP3/CMIP5 models will advance our understanding of the dynamical mechanism of the glacial climate, will add new insights into the model–data comparison at the regional scale, and will contribute to model improvements for the next PMIP/CMIP phase. Taken together, the analysis in this study for the LGM climate over China and East Asian monsoon will consider all the simulations available from the PMIP3 database to investigate the similarities and differences of the model results between the latest and previous generations of the PMIP project as well as the compatibility between simulations and reconstructions.

2. Models and data

The present study used all the nine models under the latest PMIP3/CMIP5 protocol for the LGM climate simulations, including five AOGCMs and four AOVGCMs, which have overall higher horizontal resolution than the former PMIP1/2 models. Basic information about the nine models is listed in Table 1. The boundary conditions for the LGM experiment included changes in the Earth's orbital parameters (Berger, 1978), ice-sheet extent, topography, land–sea mask, and atmospheric greenhouse gas concentrations. In PMIP3, the atmospheric concentrations of CO₂, CH₄, and N₂O decreased from the pre-industrial levels of 280 ppm, 760 ppb, and 270 ppb to 185 ppm, 350 ppb, and 200 ppb for LGM, respectively. SSTs were computed by using oceanic general

circulation models. The vegetation was fixed at the pre-industrial state in AOGCMs but was simulated with dynamic vegetation models in AOVGCMs in the pre-industrial and LGM experiments. More details about the models and experiments are provided by Taylor et al. (2012) and are available online at <http://pmip3.lsce.ipsl.fr/>.

The temperature and precipitation data used in the model evaluation were taken from the CN05.1 monthly dataset for 1961–2000, with a half-degree horizontal resolution over China, developed by the National Climate Center of the China Meteorological Administration (Wu and Gao, 2013). Wind data used to assess the ability of the models were taken from the National Centers for Environmental Prediction–National Center for Atmospheric Research (NCEP–NCAR) re-analysis of monthly meridional wind at 850 hPa with a horizontal resolution of 2.5° × 2.5° for 1979–2000 (Kalnay et al., 1996). Both kinds of data are hereafter referred to as observation for convenience. Considering that there are differences in the horizontal resolution among the models, all model and observation data were interpolated to a relatively midrange resolution of 2.5° × 2° (longitude × latitude).

3. LGM climate over China

3.1. Evaluation of climate models

Confidence on the LGM climate simulation rests largely on the reliability of the climate models to reproduce the present-day geographical pattern and magnitude of temperature and precipitation over China and of East Asian monsoon. Thus, the spatial correlation coefficient (SCC), the standard deviation, and the centered root-mean-square difference (CRMSD) of each pre-industrial experiment with respect to observation were calculated. Based on 179 grid points across mainland China, the Taylor diagram (Fig. 1) shows that the SCCs range from 0.86 to 0.99 (0.25 to 0.90) for annual and seasonal temperatures (precipitation), all of which are statistically significant at the 99% confidence level. This suggests that all nine models well simulate the geographical pattern of the observed temperature and precipitation over China. In addition, the normalized standard deviations and CRMSDs are 0.78–1.44 (0.58–1.86) and 0.21–0.71 (0.46–1.42) for the annual and seasonal temperatures (precipitation). Generally, most models can reliably reproduce the spatial pattern and variability of annual and seasonal temperatures and precipitation over China, with a larger spread for precipitation than for temperature. The best model performance is seen in autumn (September–November) [spring (March–May)] and the poorest in spring [winter (December–February)] for temperature [precipitation]. Note that most models perform better than previous PMIP1/2 models for modern temperature and precipitation conditions, as indicated from the overall higher SCCs and lower CRMSDs (Jiang et al., 2011). The median of the nine models yields an SCC of 0.96–0.98 (0.77–0.88), a normalized standard deviation of 1.05–1.20 (0.94–1.05), and a normalized CRMSD of 0.21–0.32 (0.47–0.69) for annual and seasonal temperatures (precipitation), showing quantitatively higher reliability than most of the individual models (Fig. 1). Given that the multi-model median tends to smooth the signal from poorly

Table 1
Basic information of the nine climate models within PMIP3 for the LGM experiments in this study.

Model ID	Model type	Atmospheric resolution	Length of run analyzed (year)	Data for wind at 850 hPa	
1	CCSM4	AOGCM	1.25° × ~0.9°, L26	301	√
2	CNRM-CM5	AOGCM	~1.4° × 1.4°, L31	200	
3	COSMOS-ASO	AOVGCM	3.75° × ~3.7°, L19	600	√
4	FGOALS-g2	AOVGCM	~2.8° × 3–6°, L26	100	
5	GISS-E2-R	AOGCM	2.5° × 2°, L40	100	
6	IPSL-CM5A-LR	AOVGCM	3.75° × ~1.9°, L39	500	√
7	MIROC-ESM	AOVGCM	~2.8° × 2.8°, L80	100	√
8	MPI-ESM-P	AOGCM	1.875° × ~1.9°, L47	100	√
9	MRI-CGCM3	AOGCM	1.125° × ~1.1°, L48	100	

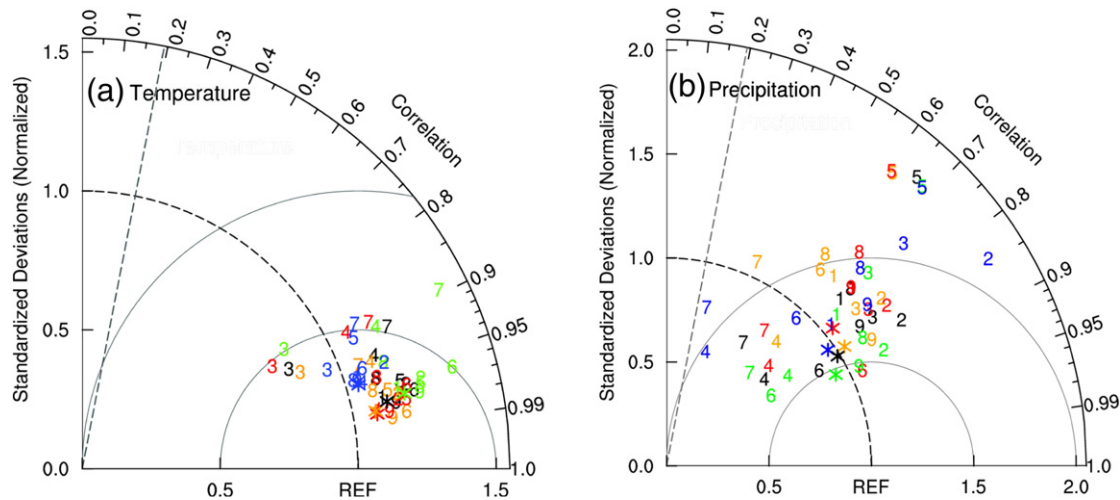


Fig. 1. Taylor diagram (Taylor, 2001) displaying the normalized pattern statistics of climatological (a) temperature and (b) precipitation over China between the nine models for the pre-industrial period and observation for 1961–2000. Numbers denote the models listed in Table 1 and asterisks represent the median of the nine models; blue, green, red, orange, and black correspond to winter, spring, summer, autumn, and the annual mean, respectively. The radial coordinate gives the standard deviation normalized by the observed value, and the angular coordinate gives the correlation with observation, with oblique dashed lines showing the 99% confidence level. The normalized CRMSD between a model and observation (marked as REF) is their distance apart.

behaving models, the median of all models is emphasized in the following analysis without further screening of the models.

3.2. Surface temperature

In response to the LGM forcing, the surface temperature decreased significantly over China relative to the pre-industrial period. The regionally averaged annual temperature decreased by 2.7–7.4 K in the nine models and by 4.3 K in their median, and the standard deviation of the nine models was 1.2 K (Fig. 2a). On the seasonal scale, all nine models reproduced colder surface temperatures during the LGM, with a decrease of 3.2–7.1 K in winter, 2.6–6.6 K in spring, 2.0–8.0 K in summer (June–August), and 3.1–7.9 K in autumn averaged over China and a standard deviation of 1.2–1.8 K for all models (Fig. 2a). The median of the nine models showed a surface cooling of 4.4 K, 3.7 K, 4.1 K, and 5.1 K for the entire China in winter, spring, summer, and autumn, respectively. At large scales, the geographical distribution of the seasonal temperature changes was generally similar to the annual mean pattern during the LGM. There is high consistency across models, as the annual and seasonal temperatures showed cooling of 2–8 K over China, with the strongest cooling occurring over the Tibetan Plateau and Northeast China (Fig. 3a, c–f).

Comparatively, the present simulated annual and seasonal cooling averaged over China during the LGM was generally similar in magnitude to that from the seven PMIP2 coupled models, stronger than that in the ten PMIP1 SST-f experiments, but slightly weaker than that from the eight PMIP1 SST-c simulations (right panel in Fig. 2a; Jiang et al., 2011), which can be attributed to the SST changes among different types of experiments. The LGM SSTs were computed by oceanic general circulation models in the PMIP2/3 simulations and by slab ocean models in the PMIP1 SST-c experiments, but they were reconstructed from CLIMAP project members (1981) for the PMIP1 SST-f experiments, contributing to different magnitudes of reductions in annual and seasonal SSTs over the western North Pacific and thus surface cooling over China during the LGM. On the other hand, the spatial pattern of the annual and seasonal cooling reproduced by the PMIP3 models was overall comparable to that in the PMIP1/2 experiments but the magnitudes differed between each other (Jiang et al., 2011).

To compare with the above simulations, we collected records of pollen, sand wedge, ice cores, mirabilite, stalagmite, paleosol, halite, peat, and brine at 124 sites across China to reconstruct the LGM annual temperature changes (Fig. 3b; Supplementary Table S1). The proxy data

suggest generally colder than present climate conditions over China, with a level of -7.0 ± 3.5 K in South China (20° – 33° N, 105° – 120° E), -6 K to -9 K over the Tibetan Plateau (28° – 37° N, 80° – 102° E), -13 K to -15 K in the Hexi Corridor (39° – 41° N, 94° – 100° E), and at least -8 K to -10 K in North and Northeast China (34° – 50° N, 105° – 135° E) (Supplementary Table S1; Jiang et al., 2011). Based on the median of the nine PMIP3 models, the LGM annual temperature decreased by 3.5 K averaged over South China, by 4.4 K over the Tibetan Plateau, by 4.1 K in the Hexi Corridor, and by 5.0 K in North and Northeast China, with an inter-model scatter of 1.1 K, 1.4 K, 1.5 K, and 2.8 K, respectively, also showing a much smaller magnitude of annual cooling (especially in the Hexi Corridor) than the proxy estimates. Overall, the annual cooling magnitudes reproduced by the PMIP3 models were similar to those in the PMIP2 experiments but weaker (stronger) than those in the PMIP1 SST-c (SST-f) simulations in the above four regions of comparison (Jiang et al., 2011). Thus, the underestimation of the annual surface cooling during the LGM from the previous PMIP1/2 experiments, as compared with the proxy data, was also seen in the latest PMIP3 simulations, indicating an overall little improvement from the PMIP2 to PMIP3 models. However, the PMIP2/3 and PMIP1 SST-c simulations with interactive ocean were in better agreement with proxy data than the PMIP1 SST-f experiments, indicating the important role of ocean dynamics in the East Asian climate during the LGM. Comparison between the PMIP2 simulations using HadCM3M2 and HadCM3M2-veg further suggested that vegetation feedback was another important process in the LGM climate (Jiang et al., 2011). In the PMIP3 simulations, the annual and seasonal surface cooling over China in the four AOVGCMs (COSMOS-ASO, FGOALS-g2, IPSL-CM5A-LR, and MIROC-ESM) was overall stronger than that in the three (CNRM-CM5, MPI-ESM-P, and MRI-CGCM3) out of five AOGCMs, which was more consistent with reconstructions, but was much weaker than that in one AOGCM (GISS-E2-R) (Fig. 2a). It should be noted that these preliminary comparisons cannot strictly diagnose the pure vegetation feedback during the LGM because the pairs of AOGCM and AOVGCM experiments should apply the same family of models and the same control experiment, as we have done for detecting the mid-Holocene vegetation feedback (Tian and Jiang, 2013). However, these simulations are not yet available in the PMIP3 database. Therefore, following the PMIP2 HadCM3M2 and HadCM3M2-veg simulations, it calls for strict experimental designs in the next PMIP project to quantify the vegetation feedback without ambiguity.

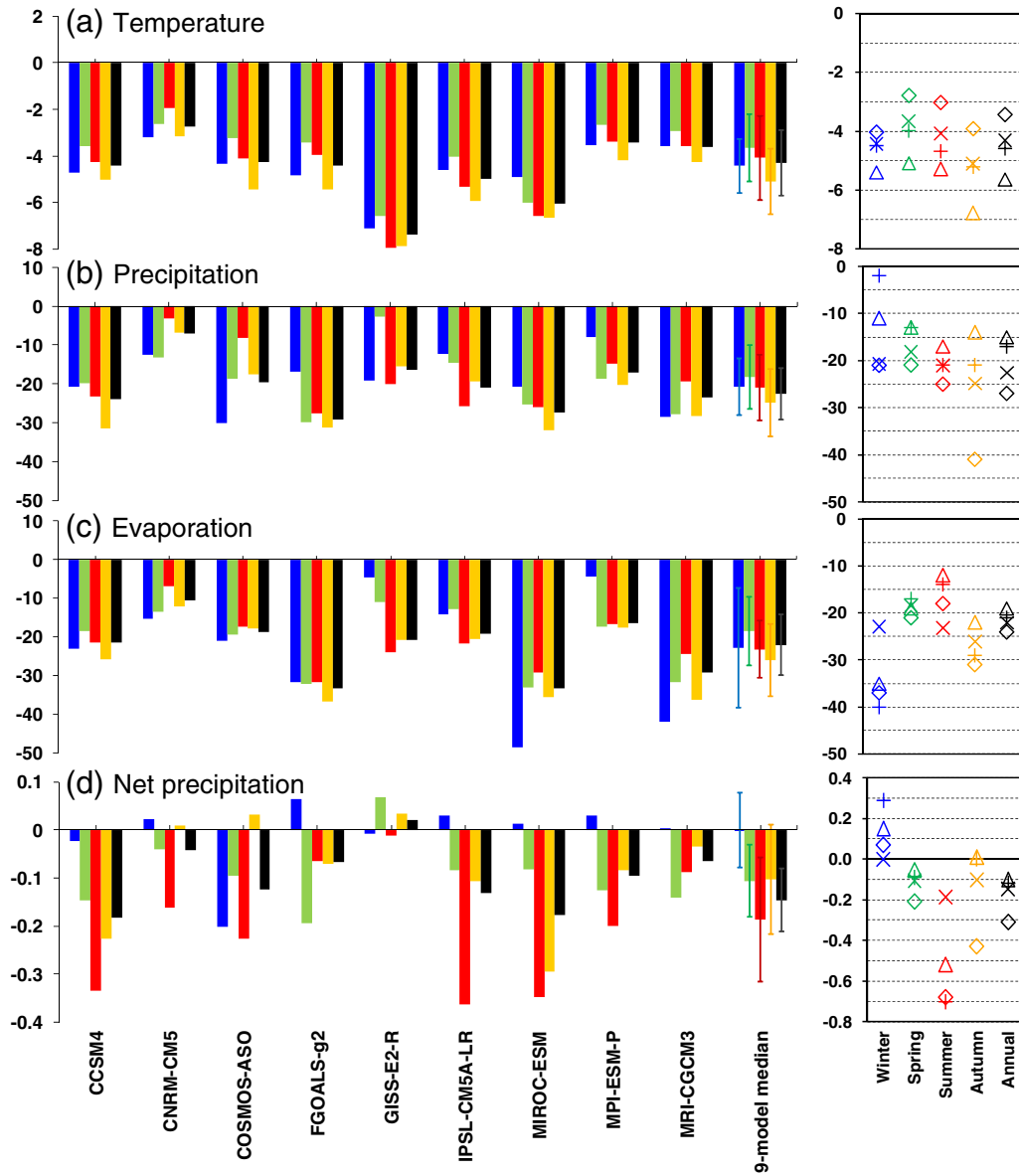


Fig. 2. LGM minus pre-industrial values of regionally averaged (a) temperature (K), (b) precipitation (%), (c) evaporation (%), and (d) net precipitation (units: mm/day) over China obtained from the nine models and their median, with (\pm) one standard deviation from the corresponding median expressed by the vertical bars. Right panels show the corresponding anomalies from the ensemble mean of the PMIP1 SST-f (diamond), PMIP1 SST-c (triangle), and PMIP2 (plus) models derived from Jiang et al. (2011) as well as from the median of the present PMIP3 models (cross). Blue, green, red, orange, and black bars (symbols) in the left (right) panels represent winter, spring, summer, autumn, and the annual mean, respectively.

3.3. Precipitation

With respect to the pre-industrial period, all nine models yielded a deficit of annual precipitation by 7–29% averaged over China during the LGM, with a median decrease of 23% and a standard deviation of 7% (Fig. 2b). Seasonal precipitation decreased by 8–30% in winter, 3–30% in spring, 3–28% in summer, and 7–32% in autumn (Fig. 2b). For the median of the nine models, the LGM precipitation change was –21%, –18%, –21%, and –25% in winter, spring, summer, and autumn, respectively, with a standard deviation of 7–9%. The geographical distribution of the annual and seasonal precipitation changes decreased by 0–50% over most parts of China during the LGM, except for the weak increase of 0–10% over the southern Tibetan Plateau in winter and spring, over Southwest China in winter, spring, and autumn, and over the coastal Southeast China in spring (Fig. 4a–e). Similar to the annual spatial pattern, the LGM decrease in seasonal precipitation was

strongest over Northwest China for all seasons, as well as over parts of Northeast and North China in winter.

When comparing the different types of experiments, the present reduction in the regionally averaged annual, spring, and autumn (winter) precipitation over China during the LGM was stronger than that in the six PMIP1 SST-c and three PMIP2 experiments but slightly weaker than (comparable to) that in the six PMIP1 SST-f simulations (right panel in Fig. 2b; Jiang et al., 2011). In summer, the present simulated precipitation decrease was comparable in magnitude to that in the PMIP2 models and was between the results of the two types of PMIP1 experiments (right panel in Fig. 2b), mainly resulted from different magnitudes in the weakening of the East Asian summer monsoon during the LGM (Jiang and Lang, 2010; Section 4.3). The large-scale change in the LGM annual and seasonal precipitation over China was similar between the different experiment types but differed in sign and magnitude at the regional scale. The present spatial pattern of annual

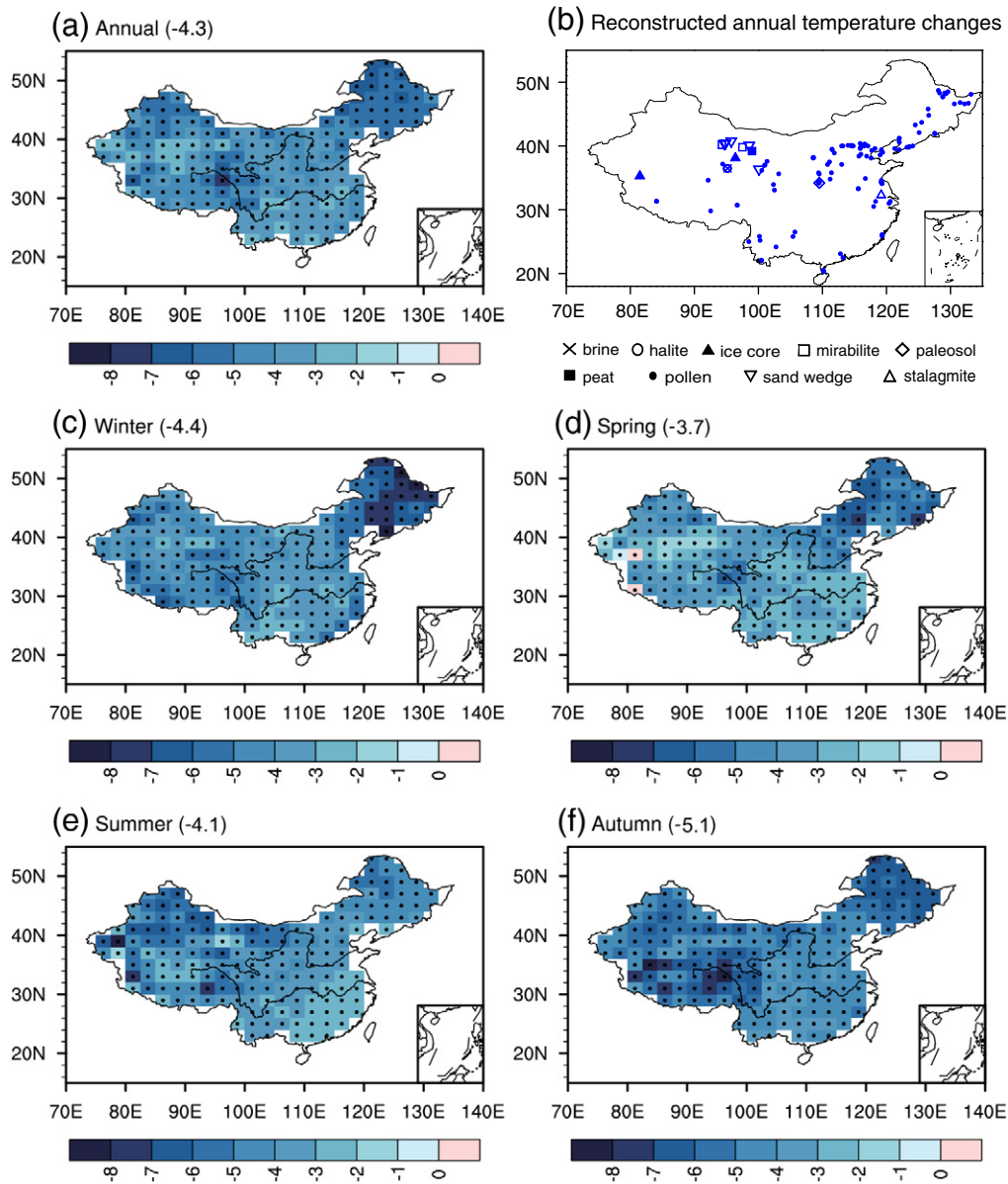


Fig. 3. LGM minus pre-industrial values of (a) annual and (c–f) seasonal temperatures (K) for the median of the nine models, with regionally averaged values over China given in parentheses. The dotted areas represent regions where at least 70% of the models share the same sign of anomaly. (b) Reconstructed annual temperature changes during the LGM relative to the present day. Blue represent colder conditions (see Supplementary Table S1 for references).

precipitation change, for example, was similar to that simulated in the PMIP2 models but slightly different from that in the PMIP1 SST-c experiments, in which annual precipitation increased in Southwest China and decreased with a weaker magnitude or even slightly increased in Xinjiang (Jiang et al., 2011).

3.4. Evaporation

Owing to the LGM surface cooling, annual evaporation consistently decreased by 11–33% averaged over China in the nine models, with a standard deviation of 8% and median decrease of 22% with respect to the pre-industrial level (Fig. 2c). Similarly, seasonal evaporation decreased by 4–49%, 11–33%, 7–32%, and 12–37% in the nine models and by 23%, 18%, 23%, and 26% for their median in winter, spring, summer, and autumn, respectively. The largest scatter across the models was seen in winter (Fig. 2c). The annual evaporation change over China was similar in spatial pattern and magnitude to the precipitation change

(Fig. 5a). Moreover, seasonal evaporation decreased by 0–50% over almost the entire country, with the magnitude being overall stronger in the west than in the east. The geographical distribution of the summer and autumn evaporation changes dominated the annual change pattern (Fig. 5).

Considering the different experiment types, the present change in the LGM evaporation averaged over China was generally comparable to that simulated by the PMIP1/2 models for the year and in spring but overall weaker (stronger) than that in the PMIP1/2 experiments in winter (summer) (right panel in Fig. 2c; Jiang et al., 2011). However, the relative change of the regionally averaged autumn evaporation over China simulated by the nine PMIP3 models was slightly stronger than that simulated by the six PMIP1 SST-c but somewhat weaker than that in the six PMIP1 SST-f and three PMIP2 experiments (right panel in Fig. 2c). These differences in the LGM annual and seasonal evaporation reduction over China among the different types of experiments were mainly related to the surface temperature anomalies.

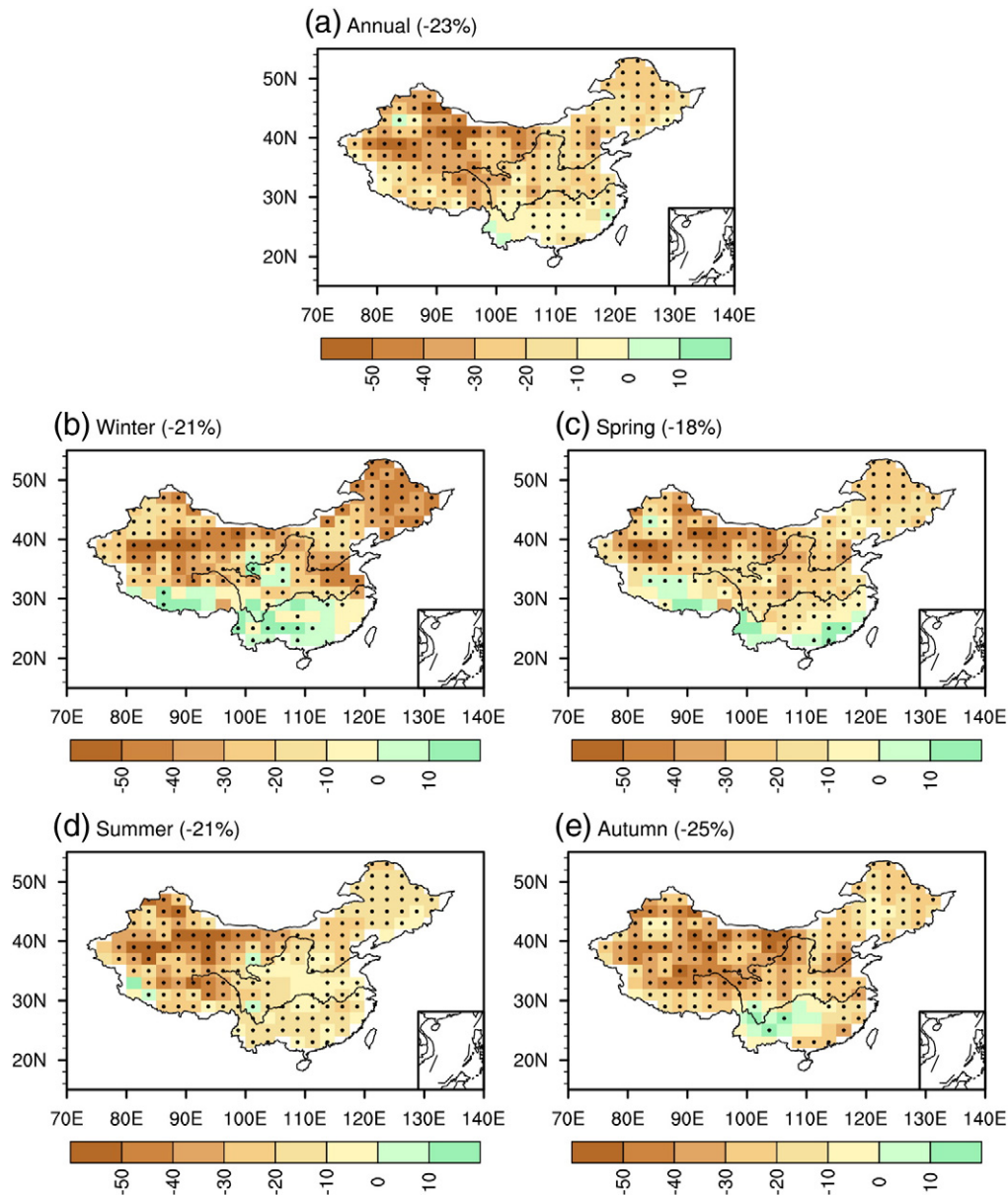


Fig. 4. Percentage changes in annual and seasonal precipitation during the LGM against the pre-industrial period for the median of the nine models. Regionally averaged percentage changes over China are given in the parentheses. The dotted areas represent regions where at least 70% of the models share the same sign of anomaly.

Moreover, the distribution of the present annual evaporation change differed from that in the PMIP1/2 simulations, in which the strongest reduction was simulated over Southeast China in the PMIP1 experiments and larger spatial variability, particularly in West and North China, was seen in the PMIP2 experiments (Jiang et al., 2011).

3.5. Net precipitation

As the LGM changes in precipitation and evaporation showed comparable values at the annual and seasonal scales, the net precipitation change over China was very small in magnitude. With respect to the pre-industrial period, the LGM annual net precipitation decreased by 0.04–0.18 mm/day in eight models but increased by 0.02 mm/day in GISS-E2-R, with a standard deviation of 0.07 mm/day and median of 0.15 mm/day averaged over China (Fig. 2d). In the median of the nine models, the spatial pattern of the annual net precipitation change yielded a decrease by 0–0.5 mm/day over most parts of the country, particularly over central and eastern China where a larger decrease was seen in annual precipitation than annual evaporation, whereas a weak

increase of 0–0.2 mm/day was seen over the western Tibetan Plateau and parts of Xinjiang and South China (Fig. 6a).

The LGM change in net precipitation averaged over the country differed in magnitude depending on the season and the model (Fig. 2d). It varied from -0.20 mm/day to 0.06 mm/day in winter, from -0.19 mm/day to 0.07 mm/day in spring, from -0.36 mm/day to -0.01 mm/day in summer, and from -0.29 mm/day to 0.03 mm/day in autumn for the nine models, with the largest standard deviation in summer. In the median of the nine models, the LGM net precipitation change was -0.001 mm/day, -0.11 mm/day, -0.19 mm/day, and -0.10 mm/day for the entire China in winter, spring, summer, and autumn, respectively, and showed large differences in the geographical distribution among seasons. In winter, the net precipitation change was less than 0.3 mm/day over most parts of China during the LGM, except for an increase of 0.3–0.5 mm/day in the southern Tibetan Plateau and South China (Fig. 6c). The LGM net precipitation change in spring and autumn was similar to the large-scale annual pattern over China (Fig. 6d and f). However, the summer net precipitation decreased by 0.3–0.5 mm/day over the southeastern

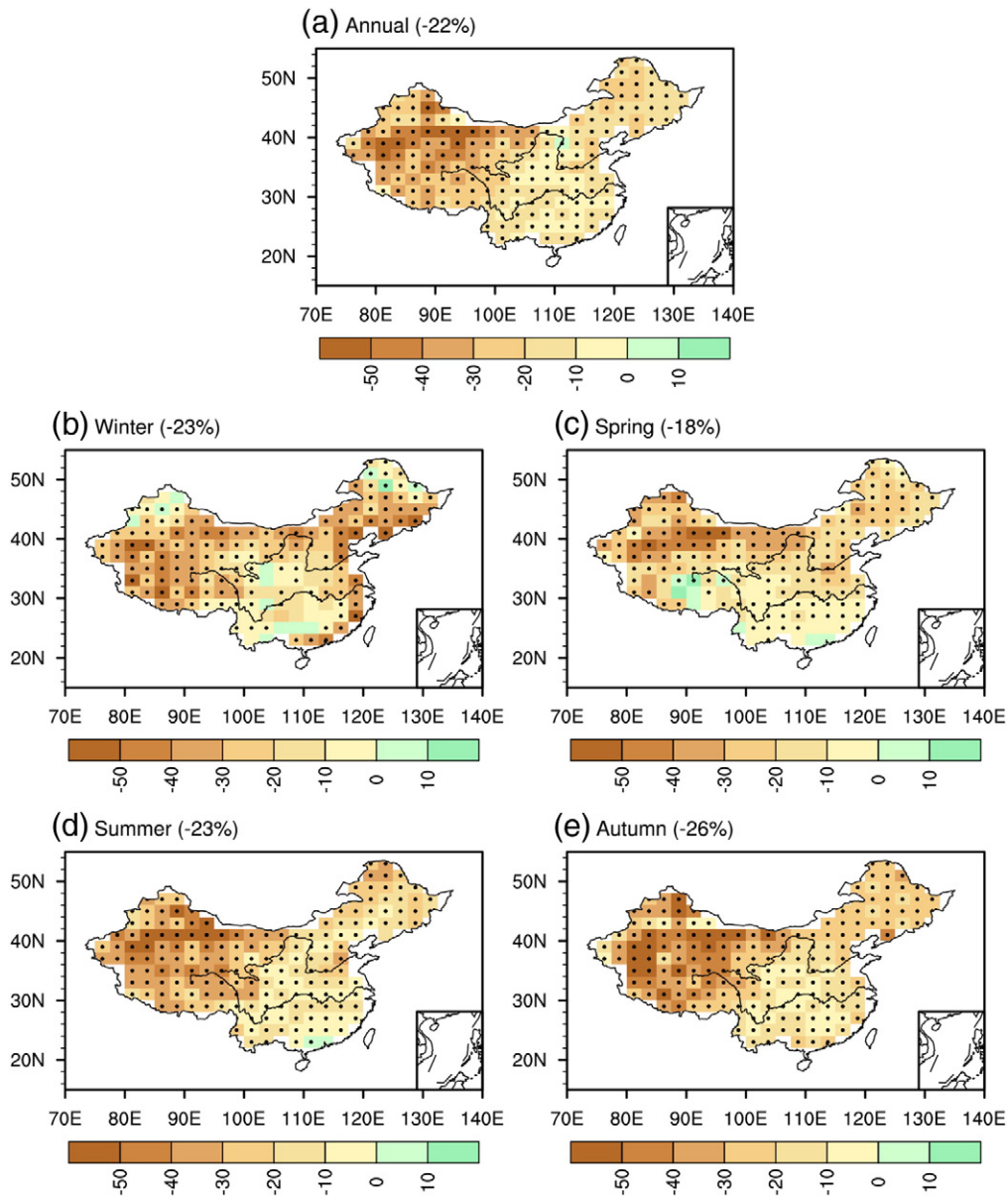


Fig. 5. Same as Fig. 4, but for evaporation.

Tibetan Plateau and most of South China but slightly increased over most of northwestern China and parts of North and Northeast China during the LGM (Fig. 6e). Thus, the LGM decrease in annual net precipitation was mainly due to the larger decrease in precipitation than evaporation in spring, summer, and autumn over China.

Among the different types of experiments, the present regionally averaged change in net precipitation over China was opposite to (weaker than) that obtained from the PMIP1/2 experiments in winter (summer), whereas it was comparable (opposite) to that simulated by the PMIP1 SST-c and PMIP2 models and weaker than the PMIP1 SST-f model values for the year and in spring (in autumn) (right panel in Fig. 2d; Jiang et al., 2011). There are similarities and differences between each of the experiment types for the spatial distribution of the LGM change in the annual net precipitation over China. The large-scale dry conditions over most parts of China were reproduced by all experiments, even though the magnitudes differed. However, the PMIP1 SST-f simulations reproduced drier conditions, whereas the other three types of experiments reproduced wetter conditions over parts of Xinjiang and South China. That was because the annual reduction in precipitation

was stronger (weaker) than in evaporation in the PMIP1 SST-f (PMIP2/3) simulations, while the annual precipitation slightly increased but annual evaporation decreased in the PMIP1 SST-c experiments over these regions (Jiang et al., 2011; Figs. 4a, 5a). Furthermore, over western Tibetan Plateau, the present simulations yielded higher annual net precipitation, whereas the other three types of experiments yielded lower (Fig. 6a; Jiang et al., 2011), which may be related to the more realistic topography in the PMIP3 models since their horizontal resolutions were overall higher than those in the previous PMIP1/2 models.

Here the collective reconstruction of annual humidity changes during the LGM was based on records of lake status, pollen, paleosol, sand wedge, mirabilite, stalagmite, halite, and peat at 128 sites over China for model–data comparison (Fig. 6b; Supplementary Table S1). The large-scale proxy data suggested that the LGM climate was drier than the present-day climate in eastern China but wetter in the western part. Qualitatively, the annual net precipitation change during the LGM based on the nine PMIP3 models was broadly consistent with the reconstructed moisture conditions over most parts of China (Fig. 6a

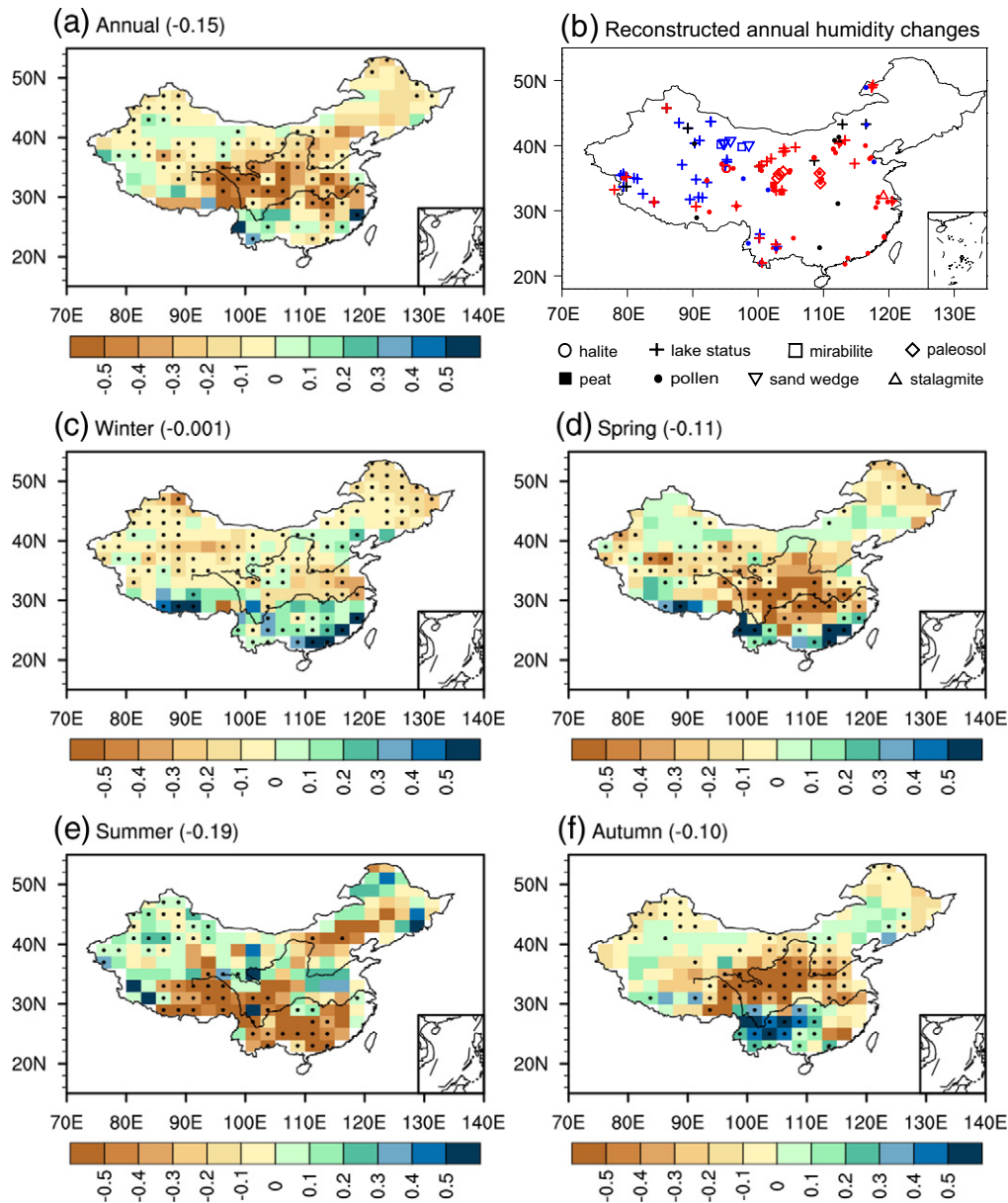


Fig. 6. LGM minus pre-industrial values of (a) annual and (c–f) seasonal net precipitation (mm/day) for the median of the nine models, with regionally averaged values over China given in parentheses. The dotted areas represent regions where at least 70% of the models share the same sign of anomaly. (b) Reconstructed annual humidity changes during the LGM relative to the present day. Red, black, and blue represent drier, normal, and wetter conditions (see Supplementary Table S1 for references).

and b), especially for the wetter conditions over the western Tibetan Plateau and Hexi Corridor where the opposite held for the 15 PMIP1/2 simulations (Jiang et al., 2011), implying an improvement of present models and the importance of reasonable description for complex topography. Similar to the PMIP1/2 results, drier conditions were simulated over the eastern Tibetan Plateau by the PMIP3 models, which agreed with the drier climate from pollen-based reconstructions (Tang et al., 1998; Wan et al., 2008) but disagreed with the wetter conditions reconstructed from lake status data during the LGM (Yu et al., 2003), with the former reconstructions more credible than the latter as discussed by Jiang et al. (2011). Both drier and wetter conditions were suggested by pollen or lake status records in Yunnan (Qin and Yu, 1998; Farrera et al., 1999; Yu et al., 2000, 2003; Herzsuh, 2006; Li and Morrill, 2013), where wetter climate was reproduced by the PMIP3 (Fig. 6a) and PMIP1 SST-c models but drier conditions in the PMIP1 SST-f and PMIP2 simulations (Jiang et al., 2011), preventing an assessment of the compatibility between simulations and reconstructions.

4. LGM East Asian monsoon

4.1. Evaluation of climate models

The East Asian monsoon is characterized by prevailing northerly winds in winter and southerly winds in summer in the lower troposphere, particularly at 850 hPa, over the East Asian continent and the western part of the western North Pacific subtropical high. Referring to previous studies (Tao and Chen, 1987; Wang et al., 2008; Jiang and Lang, 2010), the winter and summer meridional wind speed at 850 hPa based on 152 grid points within 20°–45°N and 105°–135°E was used to measure the intensity of the East Asian winter and summer monsoon, respectively, as well as the ability of the models to reproduce the present-day East Asian monsoon. For the five models with wind data available, the SCCs varied from 0.25 to 0.94 (0.06 to 0.76), with all values (all but one) being statistically significant at the 99% confidence level; the normalized

standard deviation ranged from 0.87 to 1.03 (0.67 to 2.08); and the normalized CRMSDs were 0.35–1.18 (0.66–1.82) in winter (summer). Overall, the PMIP3 models show better performance for the East Asian winter monsoon than for the summer one, and

outperform most of the PMIP1/2 models applied in Jiang and Lang (2010). Considering the limited number of climate models, the LGM East Asian monsoon changes are analyzed by model in this section.

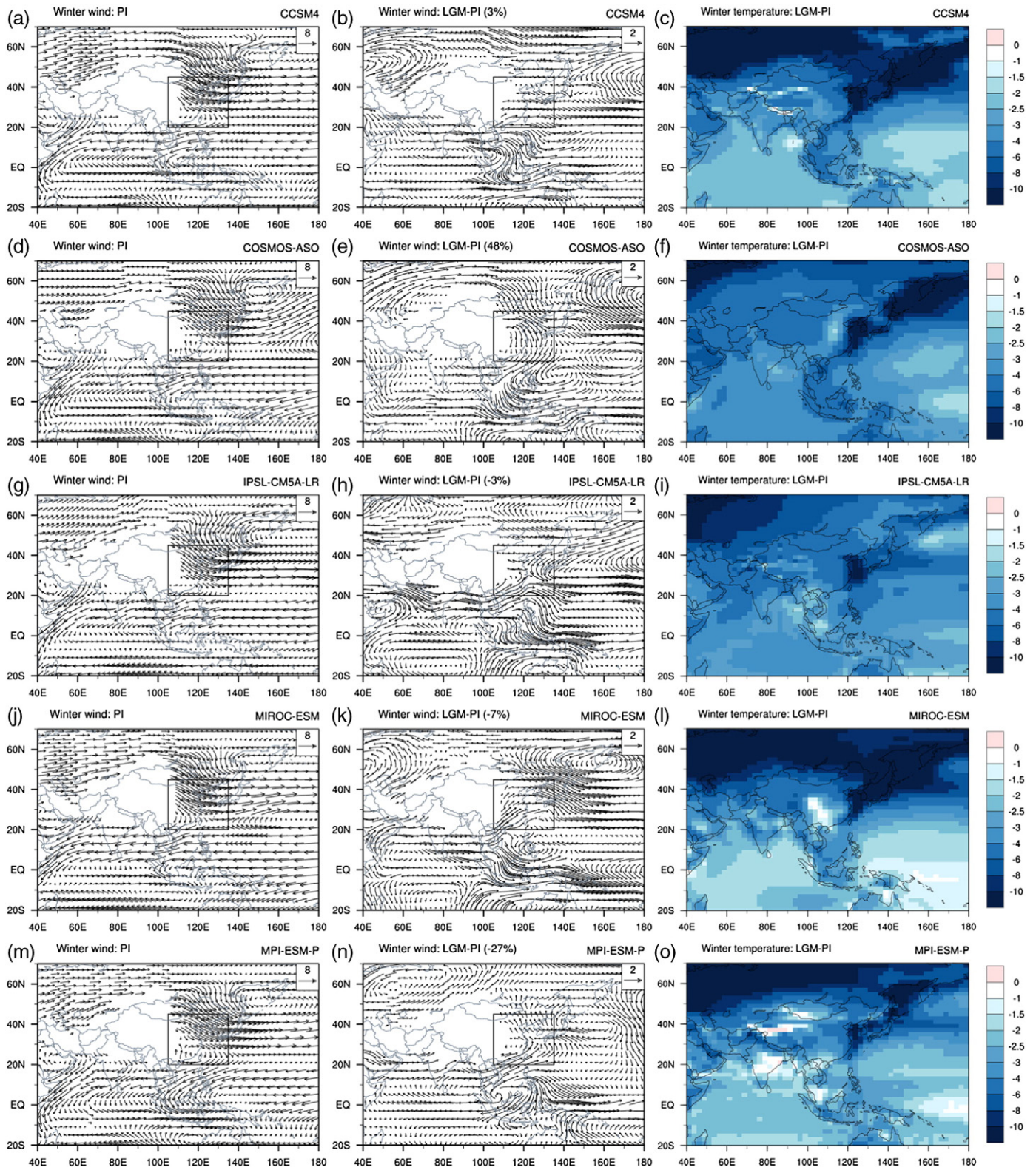


Fig. 7. Winter wind at 850 hPa (m/s) for the pre-industrial period (PI; left panel) and for the LGM minus pre-industrial (LGM – PI; middle panel) in the five models, with the corresponding percentage anomalies of the regionally averaged meridional winter wind speed within the rectangle given in parentheses. The rectangle shows the region of 25°–45°N and 105°–135°E, with regions of elevation above 1500 m left blank. Right panels show the LGM minus pre-industrial of winter temperature (K) in the models.

4.2. East Asian winter monsoon

During the LGM, the spread of the East Asian winter monsoon change is large in the five PMIP3 models. With respect to the pre-industrial period, the LGM East Asian winter monsoon intensity overall weakened by 3% in IPSL-CM5A-LR, by 7% in MIROC-

ESM, and by 27% in MPI-ESM-P, whereas it strengthened by 3% and 48% in CCSM4 and COSMOS-ASO, respectively (middle panels in Fig. 7). This is generally in line with the 21 PMIP1/2 simulations in Jiang and Lang (2010), in which the winter monsoon weakened in 11 models but strengthened in the other ten models.

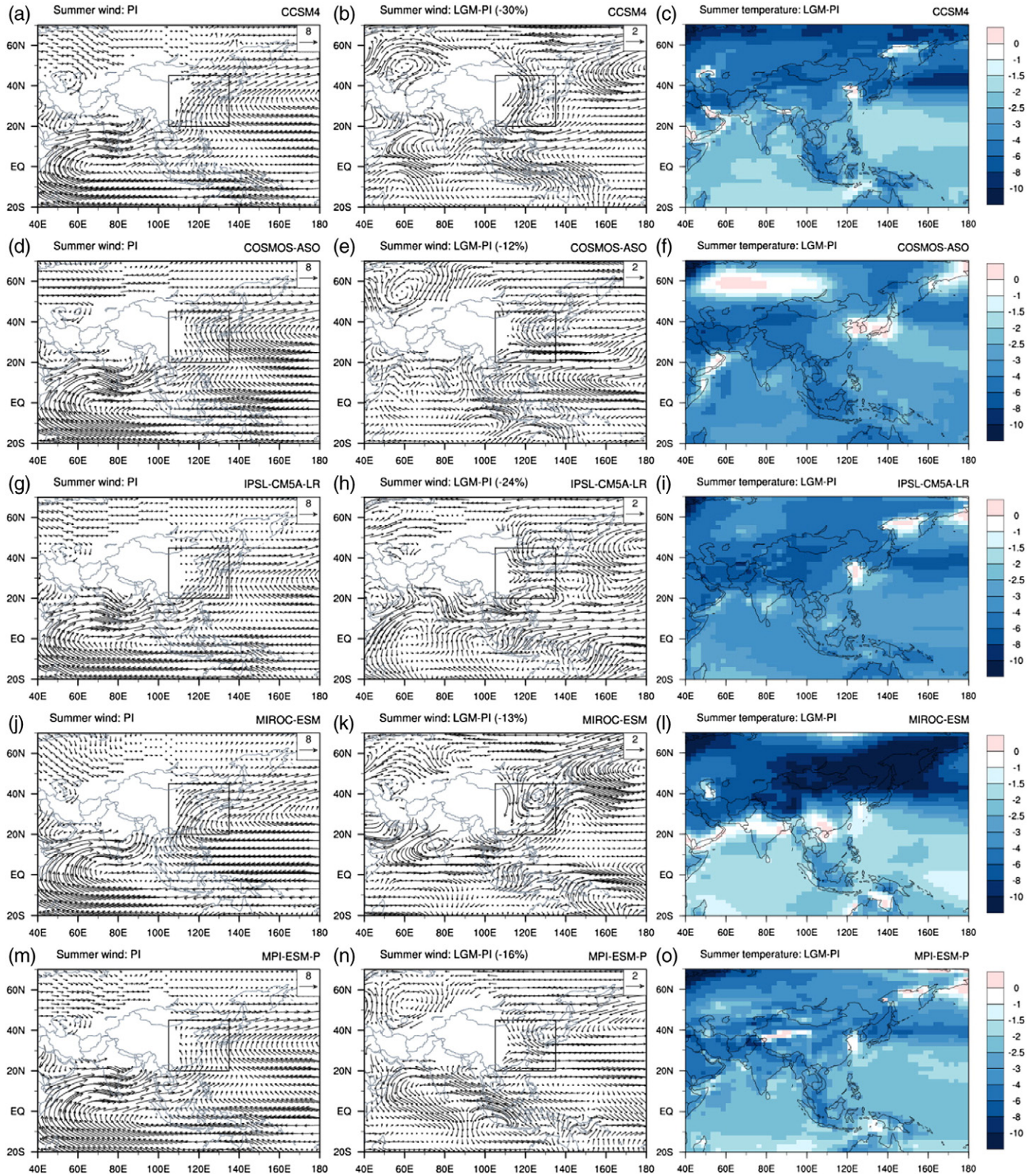


Fig. 8. Same as Fig. 7, but for summer.

The geographical distribution of the large-scale monsoon circulation at 850 hPa showed that the pre-industrial East Asian winter monsoon was characterized by prevailing northerly winds over East Asia (left panels in Fig. 7). Note that weak southerly winds occurred in southern East Asia south of about 30°N in COSMOS-ASO (Fig. 7d), opposite to the consistent northerly winds in the other four models during the pre-industrial winter. This could be mainly induced by a weak surface low-pressure center registered over the Tibetan Plateau, which was derived from relatively weaker surface cooling over there due to lower horizontal resolution in COSMOS-ASO, as compared to the other four models (Table 1). During the LGM, anomalous southerly winds consistently occurred over the East Asian continent in CCSM4, IPSL-CM5A-LR, MIROC-ESM, and MPI-ESM-P (Fig. 7b, h, k, and n), whereas the opposite was seen over the continent and adjacent oceans of East Asia in COSMOS-ASO (Fig. 7e). Such changes are due to the different spatial distributions of surface cooling between the LGM and pre-industrial periods. Strong winter surface cooling occurred over the eastern continent and the adjacent oceans of East Asia which became land during the LGM due to a sea level fall of approximately 125 m (Peltier, 1994), leading to an enhanced northeast–southwest temperature gradient between this area and the adjacent southwestern East Asia (Fig. 7c, i, l, and o). Accordingly, anomalous southerly winds were induced in the lower troposphere over the eastern continent of East Asia to compensate for the loss of atmospheric mass (Fig. 7b, h, k, and n), contributing to the weakening of the East Asian winter monsoon. In COSMOS-ASO, however, the LGM surface cooling was weaker over the southeastern than over the northwestern continent of East Asia (Fig. 7f), leading to increased southeast–northwest temperature gradient between these two regions and the strengthening of the northerly winds over the eastern parts of East Asia (Fig. 7e). Comparatively, the LGM changes in winter atmospheric circulation reproduced by the five PMIP3 models differed from those demonstrated by the 21 PMIP1/2 simulations, in which the winter monsoon overall strengthened north and weakened south of about 30°N over East Asia (Jiang and Lang, 2010).

4.3. East Asian summer monsoon

In the entire region of East Asia, the LGM summer monsoon intensity consistently weakened by 12–30% relative to the pre-industrial level in the five models (middle panels in Fig. 8), which qualitatively agreed with the weakening of the summer monsoon reconstructed from lake status data over eastern and southern Asia (Qin et al., 1998). The PMIP3 simulation was also compatible with the 14 PMIP1/2 model results, which consistently pointed to a weaker than pre-industrial East Asian summer monsoon with an averaged decrease of 25% during the LGM (Jiang and Lang, 2010).

As shown from the large-scale monsoon circulation at 850 hPa, East Asia was dominated by southerly winds during the pre-industrial period (left panels in Fig. 8). The LGM East Asian summer monsoon featured anomalous northerly winds over the continent of East Asia in CCSM4 (Fig. 8b) and IPSL-CM5A-LR (Fig. 8h), anomalous northerly winds in the north and southerly winds in the south of about 30°N in COSMOS-ASO (Fig. 8e), MIROC-ESM (Fig. 8k), and MPI-ESM-P (Fig. 8n). For the former two models, the systematic weakening of the summer monsoon circulation was consistent with that in the 14 PMIP1/2 experiments (Jiang and Lang, 2010), which was mainly due to the stronger large-scale surface cooling over the East Asian continent than over the western North Pacific (Fig. 8c and i) and thus yielded a weakened zonal land–sea thermal contrast. In the latter three models, surface cooling was generally greater in the higher latitudes than in the lower latitudes across the East Asian continent, which favored the weakening of the summer monsoon north of about 30°N over East Asia. On the other hand, the LGM surface cooling was generally weaker over the seas off the coast of the East Asian continent – especially over the Bohai Sea and the Yellow Sea, where even a warming occurred – than over the western North Pacific (Fig. 8f, l, and o). This

contributed to the increase in land–sea thermal contrast and hence sea level pressure, leading to the strengthening of the summer monsoon south of about 30°N over East Asia. Note that a weak surface warming was also seen over Korea, southern Japan and adjacent Sea of Japan as well as over the Eurasian continent (56°–62°N, 58°–80°E) in COSMOS-ASO (Fig. 8f) where the other four models showed a decreased temperature during the LGM summer (Fig. 8c, i, l, and o), mainly due to larger gains of surface heat over those regions in COSMOS-ASO than in the other four models.

5. Conclusions

In this study, the LGM climate conditions over China, including surface temperature, precipitation, evaporation, and net precipitation, as well as the East Asian winter and summer monsoons were revisited using all available climate models under the latest PMIP3/CMIP5 protocol. The main conclusions are summarized below.

- (1) During the LGM, all nine PMIP3 models reproduced colder than the pre-industrial level annual and seasonal surface temperatures over China, with an average cooling of 4.3 K, 4.4 K, 3.7 K, 4.1 K, and 5.1 K for the annual mean, in winter, spring, summer, and autumn, respectively. Such values were comparable to those obtained by the previous PMIP1/2 simulations but with different magnitudes. Compared with the multi-proxy data, the current models underestimated the annual surface cooling, as done by the PMIP1/2 models.
- (2) The LGM annual and seasonal precipitation (evaporation) over China consistently decreased in the models, with an average deficit of 18–25% (18–26%) with respect to the pre-industrial period. The LGM change in net precipitation was very small in magnitude and differed among individual models, with a median decrease of 0.10–0.19 mm/day for the annual and seasonal mean except for an overall lack of change in winter, which differed in spatial pattern and magnitude from those in the PMIP1/2 simulations. Qualitatively, the annual net precipitation change in the PMIP3 simulations was broadly consistent with the reconstructed moisture conditions over most parts of China (especially over the western Tibetan Plateau where PMIP1/2 simulations disagreed with reconstructions), except for Yunnan and the eastern Tibetan Plateau where uncertainties existed among proxy data.
- (3) The LGM East Asian monsoon change shows large spread in the PMIP3 models. Averaged over East Asia, the LGM winter monsoon weakened by 3–27% in three models but strengthened by 3–48% in the other two, while the summer monsoon consistently weakened by 12–30% in all five models. At the sub-regional scale, the winter monsoon circulation weakened (strengthened) with anomalous southerly (northerly) winds over the East Asian continent in four models (one model), and the summer monsoon circulation weakened over East Asia in two models, but weakened north and strengthened south of about 30°N in the other three models during the LGM. The spatial patterns of the LGM change in East Asian winter and summer atmospheric circulations, as simulated by the PMIP3 models, differed somewhat from those in the PMIP1/2 simulations.

Finally, it is worth mentioning that the source of the differences between simulations and reconstructions of the LGM annual temperature and moisture conditions may arise from the proxy data, the model resolution and structure, and/or the experimental design of the simulations because of the lack of dust or vegetation feedback and insufficient integration time (Masson-Delmotte et al., 2013). Thus, future work needs to move forward for the improvement of climate models as well as more reconstructions with multiple proxies and methods.

Acknowledgments

We sincerely thank the three anonymous reviewers for their insightful comments which greatly improved the paper. We also thank the climate modeling groups (listed in Table 1) for producing and making available their model output. This research was supported by the Strategic Priority Research Program (XDB03020602) of the Chinese Academy of Sciences and by the National Natural Science Foundation of China (41222034 and 41430962).

Appendix A. Supplementary data

Supplementary data to this article can be found online at <http://dx.doi.org/10.1016/j.palaeo.2016.04.020>.

References

- Bartlein, P.J., Harrison, S.P., Brewer, S., Connor, S., Davis, B.A.S., Gajewski, K., Guiot, J., Harrison-Prentice, T.L., Henderson, A., Peyron, O., Prentice, I.C., Scholze, M., Seppä, H., Shuman, B., Sugita, S., Thompson, R.S., Viau, A.E., Williams, J., Wu, H., 2011. Pollen-based continental climate reconstructions at 6 and 21 ka: a global synthesis. *Clim. Dyn.* 37, 775–802.
- Berger, A.L., 1978. Long-term variations of daily insolation and Quaternary climatic changes. *J. Atmos. Sci.* 35, 2362–2367.
- CLIMAP project members, 1981. Seasonal reconstructions of the Earth's surface at the Last Glacial Maximum. Geological Society of America Map Chart Series MC-36. Geol. Soc. Am., Boulder, Colorado.
- Farrera, I., Harrison, S.P., Prentice, I.C., Ramstein, G., Guiot, J., Bartlein, P.J., Bonnefille, R., Bush, M., Cramer, W., von Grafenstein, U., Holmgren, K., Hooghiemstra, H., Hope, G., Jolly, D., Lauritzen, S.-E., Ono, Y., Pinot, S., Stute, M., Yu, G., 1999. Tropical climates at the Last Glacial Maximum: a new synthesis of terrestrial palaeoclimate data. I. Vegetation, lake-levels and geochemistry. *Clim. Dyn.* 15, 823–856.
- Herzschuh, U., 2006. Palaeo-moisture evolution in monsoonal Central Asia during the last 50,000 years. *Quat. Sci. Rev.* 25, 163–178.
- Jiang, D., Lang, X., 2010. Last glacial maximum East Asian monsoon: results of PMIP simulations. *J. Clim.* 23, 5030–5038.
- Jiang, D., Wang, H.J., Drange, H., Lang, X., 2003. Last glacial maximum over China: sensitivities of climate to paleovegetation and Tibetan ice sheet. *J. Geophys. Res.* 108 (D3), 4102. <http://dx.doi.org/10.1029/2002JD002167>.
- Jiang, D., Lang, X., Tian, Z., Guo, D., 2011. Last glacial maximum climate over China from PMIP simulations. *Palaeogeogr. Palaeoclimatol. Palaeoecol.* 309, 347–357.
- Joussaume, S., Taylor, K.E., 1995. Status of the Paleoclimate Modeling Intercomparison Project (PMIP). In: Gates, W.L. (Ed.), *Proceedings of the First International AMIP Scientific Conference*. World Meteorol. Org., Geneva, pp. 425–430 (WCRP-92, WMO/TD-732).
- Ju, L.X., Wang, H.J., Jiang, D., 2007. Simulation of the last glacial maximum climate over East Asia with a regional climate model nested in a general circulation model. *Palaeogeogr. Palaeoclimatol. Palaeoecol.* 248, 376–390.
- Kalnay, E., Kanamitsu, M., Kistler, R., Collins, W., Deaven, D., Gandin, L., Iredell, M., Saha, S., White, G., Woollen, J., 1996. The NCEP/NCAR 40-year reanalysis project. *Bull. Am. Meteorol. Soc.* 77, 437–471.
- Li, Y., Morrill, C., 2013. Lake levels in Asia at the last glacial maximum as indicators of hydrologic sensitivity to greenhouse gas concentrations. *Quat. Sci. Rev.* 60, 1–12.
- Liu, J., Yu, G., Chen, X., 2002. Palaeoclimate simulation of 21 ka for the Tibetan Plateau and Eastern Asia. *Clim. Dyn.* 19, 575–583.
- Masson-Delmotte, V., Schulz, M., Abe-Ouchi, A., Beer, J., Ganopolski, A., González Rouco, J.F., Jansen, E., Lambeck, K., Luterbacher, J., Naish, T., Osborn, T., Otto-Bliesner, B., Quinn, T., Ramesh, R., Rojas, M., Shao, X., Timmermann, A., 2013. Information from paleoclimate archives. In: Stocker, T.F., Qin, D., Plattner, G.K., Tignor, M., Allen, S.K., Boschung, J., Nauels, A., Xia, Y., Bex, V., Midgley, P.M. (Eds.), *Climate Change 2013: The Physical Science Basis. Contribution of Working Group I to the Fifth Assessment Report of the Intergovernmental Panel on Climate Change*. Cambridge University Press, Cambridge, United Kingdom and New York, NY, USA, pp. 383–464.
- Peltier, W.R., 1994. Ice age paleotopography. *Science* 265, 195–201.
- Qin, B., Yu, G., 1998. Implications of lake level variations at 6 ka and 18 ka in mainland Asia. *Glob. Planet. Chang.* 18, 59–72.
- Qin, B., Shi, Y., Yu, G., 1998. The reconstruction and interpretations of lake status at 6 ka and 18 ka B.P. in inland mainland Asia. *Chin. Sci. Bull.* 43, 1145–1157.
- Tang, L.Y., Shen, C.M., Kong, Z.Z., Wang, F.B., Liu, K.B., 1998. Pollen evidence of climate during the last glacial maximum in eastern Tibetan Plateau (in Chinese). *J. Glaciol. Geocryol.* 20, 133–140.
- Tao, S.Y., Chen, L.X., 1987. A review of recent research on the East Asian monsoon in China. In: Chang, C.-P., Krishnamurti, T.N. (Eds.), *Monsoon Meteorology*. Oxford University Press, pp. 60–92.
- Taylor, K.E., 2001. Summarizing multiple aspects of model performance in a single diagram. *J. Geophys. Res.* 106, 7183–7192.
- Taylor, K.E., Stouffer, R.J., Meehl, G.A., 2012. An overview of CMIP5 and the experiment design. *Bull. Am. Meteorol. Soc.* 93, 485–498.
- Tian, Z., Jiang, D., 2013. Mid-Holocene ocean and vegetation feedbacks over East Asia. *Clim. Past* 9, 2153–2171.
- Wan, H.W., Tang, L.Y., Zhang, H.C., Li, C.H., Pang, Y.Z., 2008. Pollen record reflects climate changes in eastern Qaidam Basin during 36–18 ka B.P. (in Chinese). *Quat. Sci.* 28, 112–121.
- Wang, H.J., Zeng, Q.C., 1993. The numerical simulation of the ice age climate. *Acta Meteorol. Sin.* 7, 423–430.
- Wang, B., Wu, Z., Li, J., Liu, J., Chang, C.-P., Ding, Y., Wu, G., 2008. How to measure the strength of the East Asian summer monsoon. *J. Clim.* 21, 4449–4463.
- Wu, J., Gao, X.J., 2013. A gridded daily observation dataset over China region and comparison with the other datasets. *Chin. J. Geophys.* 56, 1102–1111.
- Yanase, W., Abe-Ouchi, A., 2007. The LGM surface climate and atmospheric circulation over East Asia and the North Pacific in the PMIP2 coupled model simulations. *Clim. Past* 3, 439–451.
- Yu, G., Chen, X., Ni, J., Cheddadi, R., Guiot, J., Han, H., Harrison, S.P., Huang, C., Ke, M., Kong, Z., Li, S., Li, W., Liew, P., Liu, G., Liu, J., Liu, Q., Liu, K.-B., Prentice, I.C., Qui, W., Ren, G., Song, C., Sugita, S., Sun, X., Tang, L., Van Campo, E., Xia, Y., Xu, Q., Yan, S., Yang, X., Zhao, J., Zheng, Z., 2000. Palaeovegetation of China: a pollen data-based synthesis for the mid-Holocene and last glacial maximum. *J. Biogeogr.* 27, 635–664.
- Yu, G., Chen, X., Liu, J., Wang, S., 2001. Preliminary study on LGM climate simulation and the diagnosis for East Asia. *Chin. Sci. Bull.* 46, 364–368.
- Yu, G., Xue, B., Liu, J., Chen, X., 2003. LGM lake records from China and an analysis of climate dynamics using a modelling approach. *Glob. Planet. Chang.* 38, 223–256.
- Zhao, P., Chen, L.X., Zhou, X.J., Gong, Y.F., Han, Y., 2003. Modeling the East Asian climate during the last glacial maximum. *Sci. China Ser. D* 46, 1060–1068.
- Zheng, Y.Q., Yu, G., Wang, S.M., Xue, B., Zhuo, D.Q., Zeng, X.M., Liu, H.Q., 2004. Simulation of paleoclimate over East Asia at 6 ka BP and 21 ka BP by a regional climate model. *Clim. Dyn.* 23, 513–529.
- Zhou, B., Zhao, P., 2009. Inverse correlation between ancient winter and summer monsoons in East Asia? *Chin. Sci. Bull.* 54, 3760–3767.